

Oblate Spheroidal Triboelectric Nanogenerator for All-Weather Blue Energy Harvesting

Guanlin Liu, Hengyu Guo, Sixing Xu, Chenguo Hu,* and Zhong Lin Wang*

Triboelectric nanogenerators (TENGs) provide one of the most promising techniques for large-scale blue energy harvesting. However, lack of reasonable designs has largely hindered TENG from harvesting energy from both rough and tranquil seas. In this paper, an oblate spheroidal TENG assembled by two novel TENG parts is elaborately designed for both situations. The TENG in the upper part is based on spring steel plates without other substrate materials, which makes it possible to output considerable power in rough seas and occupy small space. The TENG in the lower part consists of two copper-coated polymer films and a rolling ball which can capture small wave energy from tranquil seas. The working mechanism and output performance are systematically studied. A maximum open-circuit voltage of 281 V and a short-circuit current of 76 μ A can be achieved by one upper part, enough to charge a commercial capacitor for potential applications. More important, the proposed oblate spheroidal shell not only guarantees high sensitivity of the TENG in the lower part, but also qualifies the TENG with unique self-stabilization and low consumables for the next generation of TENGs with new structural design toward all-weather blue energy harvesting.

globe.^[4,5] However, lack of economical energy scavenging technologies has been restricting the development of large-scale blue energy harvesting. Recently, triboelectric nanogenerator (TENG) is invented as a profound new technology in converting ambient mechanical energy into electricity and attracts great attention worldwide.^[6–9] Different from electromagnetic generator, the TENG based on triboelectrification and electrostatic induction has superior advantages in light-weight, low-cost, and is suitable for harvesting mechanical energy in low oscillating frequency, which is promising to be used in energy harvesting in the ocean wave situation.^[10–12] In the past few years, TENG has been growing quickly in output performance with the efforts of over 40 research groups around the world.^[13–15] However, to build a TENG network that can harvest blue energy with both high efficiency

and durability, there are still many technical hurdles to be addressed.^[10,16,17]

Most previously reported TENGs can achieve optimal energy output in the rough seas, but they perform poorly in the halcyon seas, which is common in the actual sea.^[18,19] To expand the application of TENG in halcyon seas, a highly sensitive TENG for small water waves is indispensable. TENG shapes usually designed for blue energy harvesting are limited in sphere,^[18–20] cylinder,^[21–23] and cuboid.^[24–26] The mobile object inside these TENGs would lead to the imbalance of gravity center under the water waves, and lose its posture for optimal output performance, even the centrosymmetric sphere cannot survive due to its lack of centrosymmetric electrode pattern on its surface. Additional fixture for every TENG in a large-scale array would be intricate, and the cost would increase in the fabrication, installment, and maintenance. In short, a novel design of TENGs with self-stabilization and high sensitivity is in urgent need to further boost the TENG for blue energy dream.

Herein, for the first time we introduce the oblate spheroidal triboelectric nanogenerator (OS-TENG) elaborately designed with two novel TENG parts for all-weather blue energy harvesting. As shown in **Figure 1a**, the TENG in the upper part consists of three basic units based on spring steel plates with a pie iron to suppress, which would output substantial electricity under rough seas without coil springs support, thus it occupies less space and reduces cost tremendously. For the TENG in the lower part, due to the gentle slope at the bottom of the oblate


1. Introduction

Energy is the blood of modern civilization, but where it comes from and how we get it is something that touches all our life, which is also one of the most important interests for scientists.^[1–3] Among numerous energy sources, blue energy from the ocean is thought to be one of the most promising energy sources due to its wide distribution around the

G. L. Liu, Dr. H. Y. Guo, S. X. Xu, Prof. Z. L. Wang
School of Material Science and Engineering
Georgia Institute of Technology
Atlanta, GA 30332, USA
E-mail: zhong.wang@mse.gatech.edu

G. L. Liu, Dr. H. Y. Guo, Prof. C. G. Hu
Department of Applied Physics
State Key Laboratory of Power Transmission Equipment & System
Security and New Technology
Chongqing University
Chongqing 400044, P. R. China
E-mail: hucg@cqu.edu.cn

Dr. H. Y. Guo, Prof. Z. L. Wang
Beijing Institute of Nanoenergy and Nanosystems
Chinese Academy of Sciences
Beijing 100083, P. R. China

 The ORCID identification number(s) for the author(s) of this article can be found under <https://doi.org/10.1002/aenm.201900801>.

DOI: 10.1002/aenm.201900801

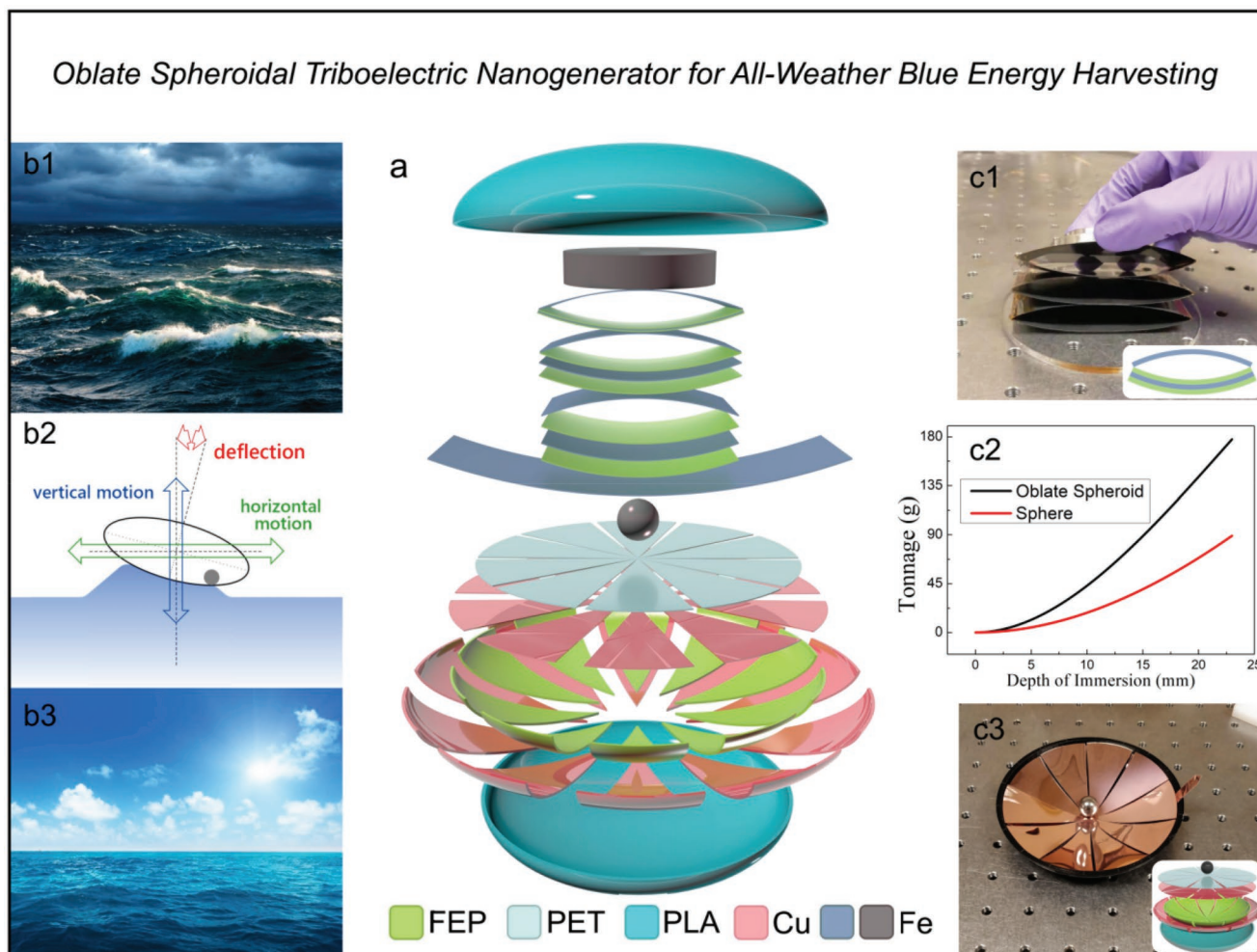


Figure 1. a) Breakdown drawing of the oblate spheroidal triboelectric nanogenerator. b) Digital photograph of two oceanic conditions: b1) rough seas, b3) halcyon seas, and b2) three basic motions of a floating TENG in them. Digital photograph of c1) the TENG in upper part and c3) the lower part; c2) the tonnage of the oblate spheroidal shell and the sphere shell with different depth of immersion. The insets are schematic diagrams of c1) a basic unit of TENG in upper part and c3) schematic diagram of the lower part.

spheroidal shell, the iron shot can reach more active area over two polymer films under small wobble, thus harvests more wave energy. The comparison of output performance between the oblate spheroidal shell and sphere shell are conducted, illustrating that the former is more suitable for scavenging large-scale blue energy in many aspects. The working mechanism and major influence factors on the output performance of both TENG parts are systematically studied. The OS-TENG can achieve a maximum open-circuit voltage of 281 V, a transferred charge per cycle of 270 nC, and a short-circuit current of 76 μ A. We believe that the OS-TENG will provide an efficient blue energy harvester toward practical applications.

2. Results and Discussion

Ocean energy harvesting should cover from rough seas to halcyon seas, as Figure 1b1,b3 shows. Since the rotation about the central axis can hardly realize by water waves due to the small size of blue energy harvesters, there are only three motions

left for the floating objects, i.e., deflection, vertical motion, and horizontal motion, as shown in Figure 1b2 and Figure S1 in the Supporting Information. For the rough sea condition, the wavelength of the water waves is short and the amplitude is large, but for the halcyon condition, the wavelength is long and the amplitude is small. Meanwhile, all three kinds of motion are violent in the rough seas, but only deflection stands out in the halcyon seas. It is hard for one TENG part to work efficiently in both situations, especially in halcyon one.

To effectively harvest the blue energy in the rough seas, the upper part of OS-TENG is composed of a pie iron and three arched triboelectric basic units. Each basic unit is made up of two jointed spring steel plates, one of which is coated with fluorinated ethylene propylene (FEP) film (Figure 1c1 and its inset). Moreover, the spring steel plates have good elasticity, flatness, a well-polished surface, and fatigue-resistance, which make it an excellent material for the construction of TENGs.^[27–29] As for the TENG in the lower part, a radial patterned FEP film coated with copper is adhered on the internal surface of the oblate spheroidal shell. A similar polyethylene terephthalate

(PET) film coated with copper is suspended above the FEP film, so the two films would separate unless the iron shot overlapped on them (Figure 1c3; Figure S2, Supporting Information). The detailed fabrication process of OS-TENG can be found in the Experimental Section. To harvest deflection energy effectively, floating on the water (not below the water) is of great importance for a TENG, because the mechanical energy of sea water mainly exists on its surface. Although an energy harvester submerged under the water can move along with the water flow, it can hardly capture the low-velocity flow motion energy and output electric energy effectively. That is why most of the reported TENGs for blue energy harvesting have to float on the water.^[18–26] So we have calculated the relation between the depth of immersion and tonnage for the oblate spheroidal shell and a sphere shell with the maximum diameter of oblate spheroidal shell. As can be seen from Figure 1c2, the oblate spheroidal shell can float on the water better than the sphere one, laying the foundation for the TENG to scavenge water wave energy from the halcyon seas. Besides that, the OS-TENG has other superior advantages.

First, according to the comparison of the oblate spheroidal shell in this work with the sphere shell with the maximum diameter of oblate spheroidal shell as shown in Figure 2, the iron shot in OS-TENG goes farther than that in sphere shell under the same slant angle (Figure 2a). Consequently, a larger touching area can be achieved by the OS-TENG with improvement of its sensitivity and output performance (Figure 2b). The detailed dimensions of the two shells are depicted in Figure S3 in the Supporting Information, where the longitudinal sections of the oblate spheroidal shell are two homocentric ellipses. The detailed calculation can be found in Note S1 in the Supporting Information. Although this advantage disappears for the TENG in the lower part under slant angle

larger than 63° , the TENG in the upper part will enter its super working state to harvest energy in the rough seas. Second, 42% of shell volume can be saved in OS-TENG compared with the sphere shell (Figure 2c), which means less material consumption, easier mass manufacture, and greater applicability for large-scale TENG arrays. The distance away from the central point under the same slant angle, coverage of iron shot under the same slant angle, and shell volume ratio in different internal heights of oblate spheroidal shell are also shown in Figure S4 in the Supporting Information, indicating the superiority of the oblate spheroidal shell. Finally, due to lack of restoring force, most previous TENGs would lose their initial postures and cannot achieve optimal output performance. The external fixture can solve the problem, yet it causes lower response and extra difficulty in device design and fabrication. As for cuboid shell TENG with a mobile object in it, it is hard for the object to recover from a lurch status, which affects the operation modes. Moreover, it depends on water wave direction, due to its nonaxial symmetry structure. As to those with cylindrical shells, the mobile objects in their TENGs tend to do circular motion around the axis and are difficult to go back to axis center of the cylinder because there is an unstable place in the center of gravity. In OS-TENG, once the iron shot rolls to one side, a torque would be formed to force the shell return to the original state (Figure 2a1), which has lower potential energy. Therefore, the oblate spheroidal shell enables the OS-TENG to possess unique self-stabilization, distinguishing itself from all other previous TENGs.

The triboelectrification and electrostatic induction are the two fundamental effects for a TENG. The two TENG parts in OS-TENG are all working in contact–separation mode, which is good for long-term operation. The electrons would transfer and remain on the surface of FEP films due to their strong

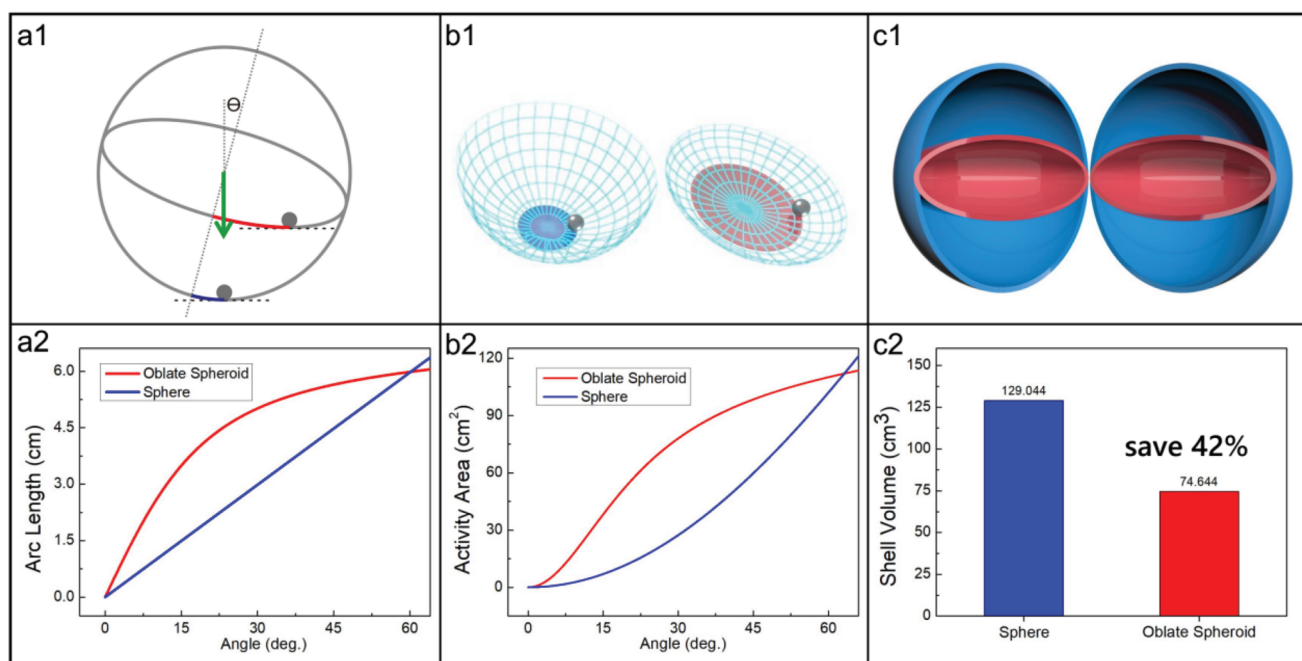


Figure 2. Comparison of the oblate spheroidal shell (marked in red) with sphere (marked in blue) in a) distance away from the central point under the same slant angle, b) coverage area of the iron shot under the same slant angle, and c) the shell volume.

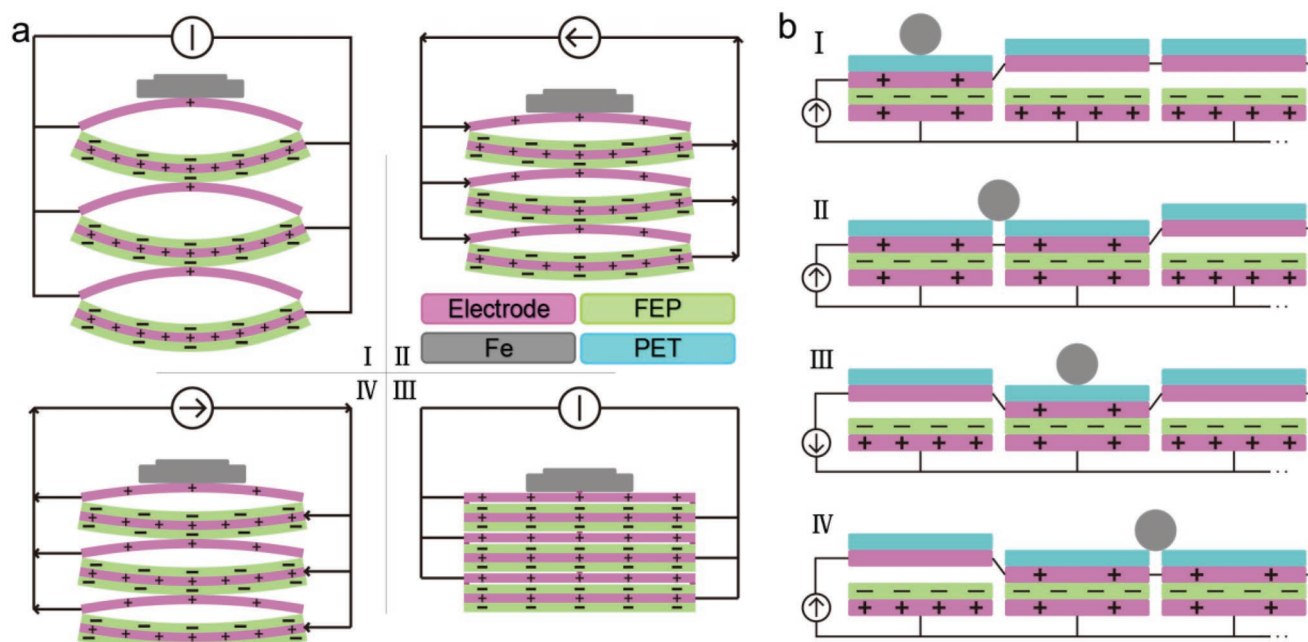


Figure 3. Working principle of TENG in a) upper part and b) lower part of OS-TENG. The arrows in the circles represent the direction of current.

electron gain capacity under the friction between Cu/Fe and FEP. After having been shaken for several times, the stable charge distribution can be achieved as shown in **Figure 3a,b**. A detailed illustration of the charge distribution procedure can be found in Figures S5 and S6 in the Supporting Information. The arrows in the circles represent the directions of the current. The working mechanism of the TENG in the upper part is shown in **Figure 3a**, when the pie iron presses the FEP film to contact the spring steel plate, the negative charge on FEP film would produce an electric potential difference between the two electrodes, driving free electrons to flow from the electrode without FEP to another electrode. Once the pie iron goes up, the separation of two electrodes would introduce a contrary electric potential difference, leading electrons to flow back. Under the reciprocating motion of the pie iron, alternating current in the external circuit can be received. **Figure 3b (I–IV)** presents the working mechanism for the sectors of TENG in the lower part. Similarly, when the iron shot moves on the sector layers and pushes the FEP film and the metal electrode to contact (iron shot on them) or separate (iron shot off them), the electric potential difference between the two electrodes drives free electrons to flow from one electrode to another, causing alternating current in the external circuit. To assess the impact of the negative charge accurately, Comsol Multiphysics soft based on the finite-element simulation has been applied to both TENG parts for electric potential distribution in the open-circuit condition, and the results in Figures S7 and S8 in the Supporting Information further verify the above analysis.

To better understand the behavior of OS-TENG under different external mechanical stimulations, the TENG in the upper part is stuck on an acrylic platform fixed on a linear motor that can produce uniform variable rectilinear motion in the vertical direction. Electric output performance under various displacement amplitudes and impel frequencies have been measured,

as illustrated in **Figure 4**, where all 3D graphs are smoothed by bilinear interpolation algorithm to be easily understood. Every two 2D graphs corresponding to a 3D graph exhibit the output performance precisely under various conditions. As shown in these graphs, except for some points, the electric output, including the transferred charge quantity per cycle, the open-circuit voltage, and the short-circuit current, increases significantly with the increase in amplitude and frequency. The maximum electric output is located at the amplitude of 12.5 mm and frequency of 4 Hz, showing a transferred charge of 270 nC, open-circuit voltage of 281 V, and short-circuit current of 76 μ A, respectively. The maximum output waveform graphs are displayed in **Figure S9** in the Supporting Information. With larger displacement amplitude input, the frictional layers would separate more sufficiently, which means an increase in the frictional active area, leading to the improvement of output performance. The rise in frequency would raise the climb acceleration of the pie iron, and the same effect can be obtained on the output performance by rising velocity and displacement. The output power of the top part under varying external resistance has been measured and provided in **Figure S10** in the Supporting Information (the input conditions fixed on amplitude of 12.5 mm and frequency of 2.5 Hz). It is obvious to see that the output power goes up sharply at first and then drops slightly as the resistance increases, reaching the maximum of 475 μ W with the matching resistance of 8 M Ω .

The output behavior of the TENG in the lower part is another vital part of OS-TENG for blue energy harvesting in the halcyon seas. Since the random motion of the iron shot under ocean agitations can be divided into two directions: radial direction and tangential direction, the measurement is carried out in these two directions. For the radial direction, the TENG in the lower part is fixed on the linear motor that provides uniform variable rectilinear motion in the horizontal

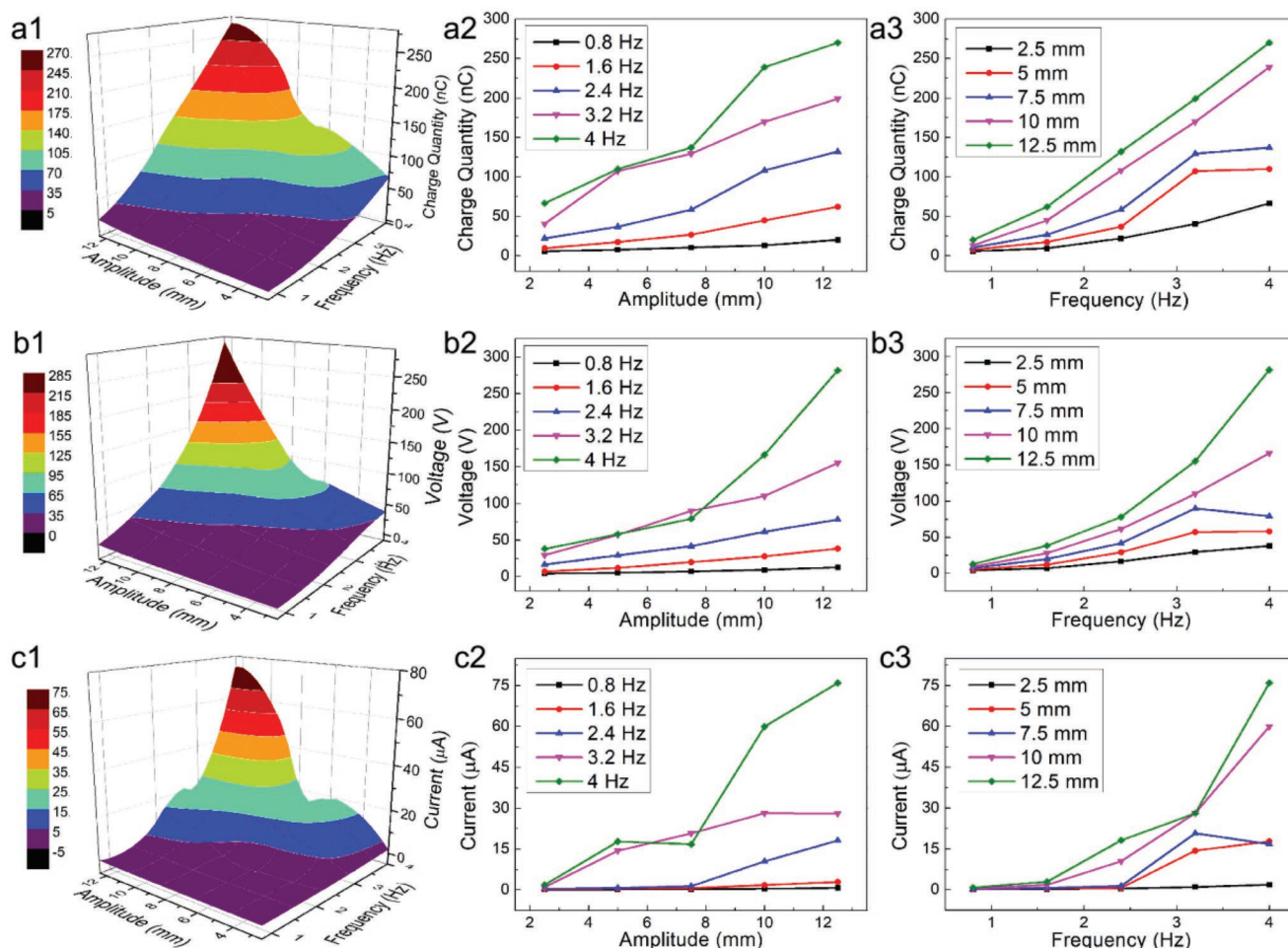


Figure 4. Electric characterization of the upper part TENG by a linear motor. 3D surface graph of the a1) transferred charge quantity per cycle, b1) open-circuit voltage, and c1) output short-circuit current versus both the frequency and amplitude. a2,a3,b2,b3,c2,c3) Corresponding 2D graphs derived from the 3D surface graph.

direction. We change the acceleration with equal difference while keep the amplitude at 20 mm during the measurement. The results in **Figure 5a–c** reflect that the output open-circuit voltage, the transferred charge quantity, and the short-circuit current increase monotonously with the increase in the acceleration. The maximum voltage of 21 V and charge quantity of 10 nC can be obtained at the acceleration of 1 m s^{-2} . It is easy to understand that the iron shot would bring more frictional area to contact/separate with higher acceleration, resulting in higher output performance. It can be seen from **Figure 5a,b** that the curves do not go back to zero at times. This is due to the mismatching frequency of the motor and the iron shot pendulum-like motion in the shell, which causes the irregular reciprocating motion of iron shot and brings frictional area from other sectors to contact/separate. For the tangential direction motion, we fix the TENG in the lower part on rotary motor coaxially and connected the two electrodes via an electric brush. The measurement of the output is conducted under different rotate speeds and slant angles, which is achieved by leaning the motor by several wedges with specific angles. The detailed data are shown in **Figures S11–S13** in the Supporting Information. Owing to the imperfect symmetry of frictional layer sectors, the

wave does not have a stable baseline, so we drew some typical section out of them and pieced them together to be a full graph. A rising trend of output emerges with the increase in the rotate speed and slant angle. To illustrate it more clearly, we connected two electrodes with a bridge rectifier and charged a capacitor ($1 \mu\text{F}$), and the charging voltages under different input conditions are depicted in **Figure 5d,e**. Short-circuit current of lower part TENG in tangential circular motion under slant angle with the same rotate speed of 40 rpm is shown in **Figure 5f**. Higher rotate speed means more frictional layer area contact/separate per second, and more transferred charge provided by the lower part. Besides, the increase in slant angle would drive the iron shot farther from the center and bring more frictional layer area to contact/separate. All these efforts above would lead to a faster charging speed in the end.

The TENG in the upper part placed on the crossgirder over the TENG in the lower part inside the oblate spheroidal shell is assembled into an OS-TENG, as exhibited in **Figure 6a**. The network of OS-TENG does not only maintain its stability without an external frame, but also harvest substantial power energy from the ocean in all-weather. For potential large-scale application of OS-TENG, we envision a future of blue energy

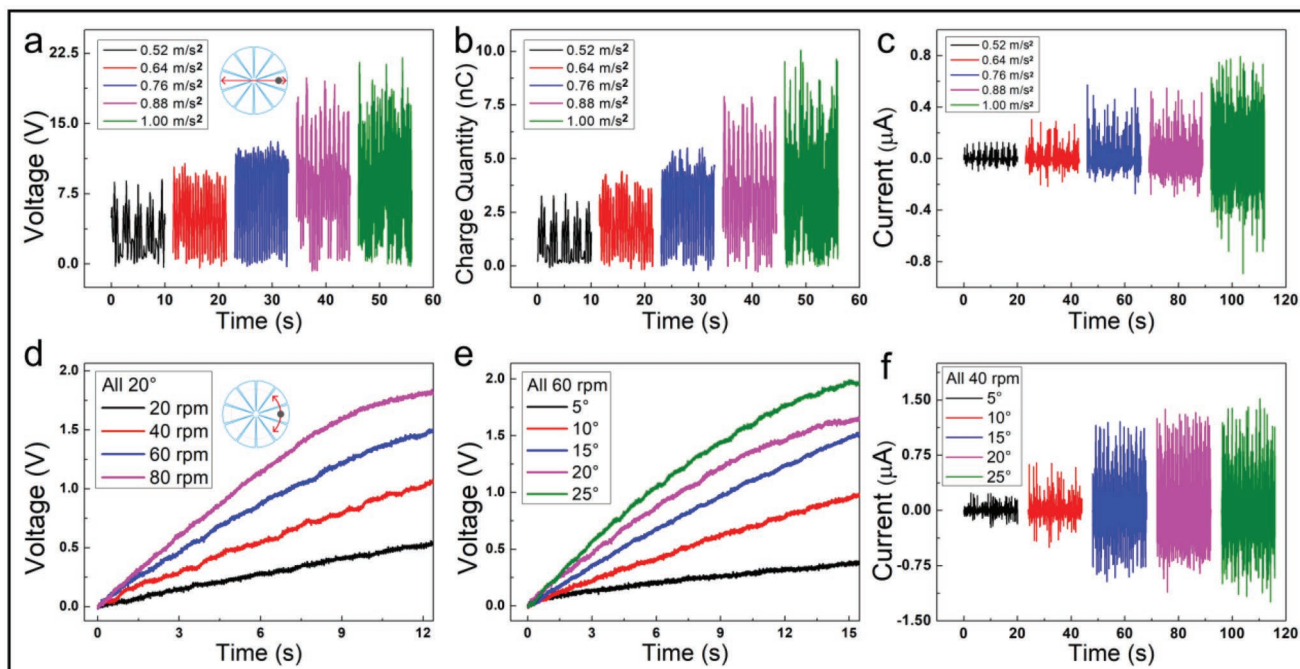


Figure 5. Electric characterization of the lower part TENG. a) Output open-circuit voltage, b) transferred charge quantity, and c) short-circuit current of lower part TENG while the iron shot in radial reciprocating motion with different accelerations of linear motor. Charging performance of lower part TENG to a capacitor while the iron shot in tangential circular motion with d) different rotate speeds and e) slant angles. f) Short-circuit current of lower part TENG in tangential circular iron motion under different slant angles with the same rotate speed of 40 rpm.

harvesting around buoys (Figure 6b). To test the performance of an OS-TENG in the water, a water tank and a vibration generator is used to generate water waves. The water tank is placed

on three round tubes so it can be pushed back and forth by a vibration generator fixed on the outer wall (Video S1, Supporting Information). The imposed motion to the tank is at frequency of

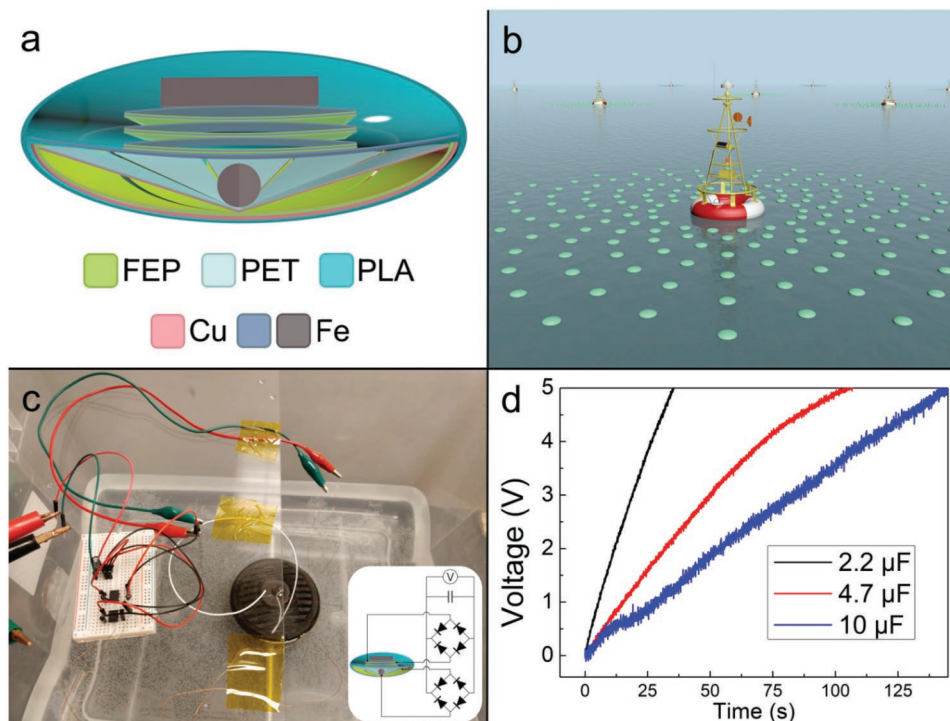


Figure 6. a) Schematic structured of an integrated OS-TENG. b) Imaginary picture of future large-scale TENG networks based on OS-TENG for blue energy harvesting. c) Digital photograph of an OS-TENG floating on the water to charge a capacitor and d) the charging voltage of capacitors with different capacitance.

2 Hz and amplitude of 20 mm. The output open-circuit voltage, the transferred charge quantity per cycle, and the short-circuit current of the upper part TENG is about 72 V, 81 nC, and 4 μ A, respectively (Figure S13, Supporting Information). This roughly accords with test data above since the pie iron inside of the upper part TENG has nearly 15 mm space in height. Besides, the pie iron in the sealed OS-TENG would not have the same sinusoidal motion as the previous tests using linear motor due to the cap of the oblate spheroidal shell. The output electricity can be used to charge different commercial capacitors, and the charging curve is depicted in Figure 6d, in which the 4.7 μ F capacitor can be charged to 5 V within 2 min while the 10 μ F capacitor needs 150 s. It only takes 35 s to charge the 2.2 μ F capacitor to 5 V.

3. Conclusion

In summary, for the first time we present the oblate spheroidal TENG based on two novel TENG parts for all-weather blue energy harvesting. The different TENG parts work on two major oceanic conditions, rough or halcyon seas, to harvest blue energy. The oblate spheroidal shell and traditional sphere shell are compared and we have proved that the oblate spheroidal shell has superior characteristics, such as high response in small agitations, self-stabilization, and low consumables. The output behavior under different input conditions is studied comprehensively to obtain a thorough understanding of those two TENG parts. A maximum open-circuit voltage of 281 V and a short-circuit current of 76 μ A can be achieved by one single upper part. We also use the OS-TENG to generate electricity by harvesting energy from the water wave and used the electricity to charge a commercial capacitor. This study provides a novel shell structure that might inspire new designs for TENGs with the similar unique characteristics for blue energy harvesting.

4. Experimental Section

Fabrication of the Oblate Spheroidal Triboelectric Nanogenerator: The hemi-oblate spheroidal shells made of polylactic acid (PLA) were prepared by a 3D printer based on the parameters in Figure S3 in the Supporting Information. For the lower part TENG, a 50 μ m thick fluorinated ethylene propylene film and a 100 μ m polyethylene terephthalate film were cleansed with ethanol and dried by air gun. The two films shown in Figure 1c3 were fabricated using a laser cutting machine (Universal Laser Systems PLS6MW) to cut a radial pattern right after two polymer films were deposited with a copper layer on the surface as an electrode by magnetron sputtering. The more precise parameter of the pattern can be seen in Figure S15 in the Supporting Information. Then, the FEP film was attached on the inner side of a hemi-oblate spherical shell by instant-bonding adhesive, and the central part of the PET film was attached uniformly on the central part of the FEP film. Two copper wires were connected to these films on the edge respectively to work as external electrodes, which could output electricity with an iron shot (12 mm in diameter) rolling on the polymer films. For the upper part, the commercial spring steel tape (Kobetool, Germany, 50 mm in width and 0.08 mm in thickness) was calcined at 350 $^{\circ}$ C for 3 h and rolled in a 500 mL beaker with a radius of 95 mm and cooled in room temperature, thus shaped in a curve with a radius of \approx 200 mm and served as springs and electrodes in upper part TENG. Then it was cut into six slices with the same lengths of 80 mm, followed by ethanol spray treatment to remove any oil contamination. Six arched slices

with curvature radius of \approx 180 mm were obtained, three of which were attached to FEP film (89.9 μ m in thickness) on both sides and each were jointed with a bared slice on both ends to form a basic close arched unit for the upper part (inset in Figure 1c1). Three basic close arched units piled up together by a double faced adhesive tape in the adjacent top. These slices with FEP film were connected together by copper wires to act as an electrode for the upper part, while the bared slices were similarly connected to act as another electrode. Combined with a pie iron (48.9 mm in diameter and 9 mm in height) on the top, the TENG in the upper part could harvest the horizontal motion energy from the ocean effectively and convert it into electricity.

To ensure that the two triboelectric nanogenerators function well and maximize the use of space inside the oblate spheroid, a spring steel plate (122 mm \times 50 mm \times 0.08 mm) with two ends fixed on the edge of hemi-oblate spheroid served as crossgirder, above which was the upper part TENG, while the iron shot could roll freely under the crossgirder (Figure 6a). The waterproofing and sealing are necessary for a blue wave energy harvester. Uniform mixture of part A and part B of tile cement in the volume ratio of 1:1 was applied to the edge of two hemi-oblate spheroidal shells for sealing. A tiny hole was tapped on the top to let the four copper wires out and then sealed by the same tile cement. The total weight of the sealed TENG was about 195 g, which could flow on the water and harvest the surface mechanical energy effectively as demonstrated in Figure 1c2.

For electric measurement of the triboelectric nanogenerator parts and OS-TENG, Keithley 6514 system electrometer was used to measure the short-circuit current, the open-circuit voltage, and the transferred charge. Before sealing, a linear motor (LinMot Linear Guide H-30) provided uniform variable rectilinear motion in vertical and horizontal directions for the upper part and the lower part, respectively. As to the tilted rotation test, the TENG in the lower part combined with the hemi-oblate spheroidal shell was fixed on the rotating motor coaxially via an acrylic circular disk, which was equipped with two electric brushes. After being sealed, the OS-TENG was placed into a water tank, which was placed on three rollable round pipes, thus a vibration generator can impel vibration to the tank. A nylon wire connected both the OS-TENG and the acrylic plate on the tank to make sure the OS-TENG would not hit the tank wall, as shown in Figure 6c. It was made sure that most of the time the nylon wire was at relaxation condition.

Supporting Information

Supporting Information is available from the Wiley Online Library or from the author.

Acknowledgements

G.L.L., H.Y.G., and S.X.X. contributed equally to this work. This research was supported by the Hightower Chair Foundation and NSFC (51572040) and the Fundamental Research Funds for the Central Universities (2018CDQYWL0046, 2019CDXZWL001). The authors also acknowledge the China Scholarship Council for supporting research at the Georgia Institute of Technology.

Conflict of Interest

The authors declare no conflict of interest.

Keywords

blue energy, oblate spheroidal, triboelectric nanogenerators

Received: March 11, 2019

Revised: May 5, 2019

Published online:

- [1] M. I. Qureshi, A. M. Rasli, K. Zaman, *J. Cleaner Prod.* **2016**, *112*, 3657.
- [2] K. W. J. Barnham, M. Mazzer, B. Clive, *Nat. Mater.* **2006**, *5*, 161.
- [3] J. Q. Jiao, Y. Li, W. F. Shen, S. S. Gai, J. G. Tang, Y. Wang, L. J. Huang, J. X. Liu, W. Wang, L. A. Belfiore, *Sci. Bull.* **2018**, *63*, 216.
- [4] J. Falnes, *Mar. Struct.* **2007**, *20*, 185.
- [5] Z. L. Wang, *Nature* **2017**, *542*, 159.
- [6] F. R. Fan, Z. Q. Tian, Z. L. Wang, *Nano Energy* **2012**, *1*, 328.
- [7] Z. L. Wang, J. Chen, L. Lin, *Energy Environ. Sci.* **2015**, *8*, 2250.
- [8] Z. L. Wang, *Nano Energy* **2018**, *54*, 477.
- [9] H. Y. Guo, X. J. Pu, J. Chen, Y. Meng, M. H. Yeh, G. L. Liu, Q. Tang, B. D. Chen, D. Liu, S. Qi, C. S. Wu, C. G. Hu, J. Wang, Z. L. Wang, *Sci. Rob.* **2018**, *3*, eaat2516.
- [10] Z. L. Wang, T. Jiang, L. Xu, *Nano Energy* **2017**, *39*, 9.
- [11] B. B. Zhang, J. Chen, L. Jin, W. L. Deng, L. Zhang, H. T. Zhang, M. H. Zhu, W. Q. Yang, Z. L. Wang, *ACS Nano* **2016**, *10*, 6241.
- [12] L. Jin, W. L. Deng, Y. C. Su, Z. Xu, H. Meng, B. Wang, H. P. Zhang, B. B. Zhang, L. Zhang, X. B. Xiao, M. H. Zhu, W. Q. Yang, *Nano Energy* **2017**, *38*, 185.
- [13] L. Zhang, B. B. Zhang, J. Chen, L. Jin, W. L. Deng, J. F. Tang, H. T. Zhang, H. Pan, M. H. Zhu, W. Q. Yang, Z. L. Wang, *Adv. Mater.* **2016**, *28*, 1650.
- [14] Z. M. Lin, J. Chen, X. S. Li, Z. H. Zhou, K. Y. Meng, W. Wei, J. Yang, Z. L. Wang, *ACS Nano* **2017**, *11*, 8830.
- [15] J. Chen, H. Y. Guo, J. G. Zheng, Y. Z. Huang, G. L. Liu, C. G. Hu, Z. L. Wang, *ACS Nano* **2016**, *10*, 8104.
- [16] Z. L. Wang, *Mater. Today* **2017**, *20*, 74.
- [17] U. Khan, S. W. Kim, *ACS Nano* **2016**, *10*, 6429.
- [18] L. Xu, T. Jiang, P. Lin, J. J. Shao, C. He, W. Zhong, X. Y. Chen, Z. L. Wang, *ACS Nano* **2018**, *12*, 1849.
- [19] T. X. Xiao, X. Liang, T. Jiang, L. Xu, J. J. Shao, J. H. Nie, Y. Bai, W. Zhong, Z. L. Wang, *Adv. Funct. Mater.* **2018**, *28*, 1802634.
- [20] X. F. Wang, S. M. Niu, Y. J. Yin, F. Yi, Z. You, Z. L. Wang, *Adv. Energy Mater.* **2015**, *5*, 1501467.
- [21] L. Feng, G. L. Liu, H. Y. Guo, Q. Tang, X. J. Pu, J. Chen, X. Wang, Y. Xi, C. G. Hu, *Nano Energy* **2018**, *47*, 217.
- [22] X. Y. Li, J. Tao, X. D. Wang, J. Zhu, C. F. Pan, Z. L. Wang, *Adv. Energy Mater.* **2018**, *8*, 1800705.
- [23] H. Y. Shao, P. Cheng, R. X. Chen, L. J. Xie, N. Sun, Q. Q. Shen, X. P. Chen, Q. Q. Zhu, Y. Zhang, Y. N. Liu, Z. Wen, X. H. Sun, *Nano-Micro Lett.* **2018**, *10*, 54.
- [24] L. Xu, Y. K. Pang, C. Zhang, T. Jiang, X. Y. Chen, J. J. Luo, W. Tang, X. Cao, Z. L. Wang, *Nano Energy* **2017**, *31*, 351.
- [25] T. Jiang, L. M. Zhang, X. Y. Chen, C. B. Han, W. Tang, C. Zhang, L. Xu, Z. L. Wang, *ACS Nano* **2015**, *9*, 12562.
- [26] H. Y. Shao, Z. Wen, P. Cheng, N. Sun, Q. Q. Shen, C. J. Zhou, M. F. Peng, Y. Q. Yang, X. K. Xie, X. H. Sun, *Nano Energy* **2017**, *39*, 608.
- [27] G. L. Liu, J. Chen, Q. Tang, L. Feng, H. M. Yang, J. Li, Y. Xi, X. Wang, C. G. Hu, *Adv. Energy Mater.* **2018**, *8*, 1703086.
- [28] G. L. Liu, H. Y. Guo, L. Chen, X. Wang, D. P. Wei, C. G. Hu, *Nano Res.* **2016**, *9*, 3355.
- [29] G. L. Liu, R. P. Liu, H. Y. Guo, Y. Xi, D. P. Wei, C. G. Hu, *Adv. Electron. Mater.* **2016**, *2*, 1500448.